




Dynamical properties of neuromorphic Josephson junctionsD. Chalkiadakis *Department of Physics, University of Crete, 71003 Herakleio, Greece*J. Hizanidis **Department of Physics, University of Crete, 71003 Herakleio, Greece
and Institute of Applied and Computational Mathematics,
Foundation for Research and Technology-Hellas, 70013 Herakleio, Greece* (Received 28 January 2022; revised 2 June 2022; accepted 14 September 2022; published 17 October 2022)

Neuromorphic computing exploits the dynamical analogy between many physical systems and neuron biophysics. Superconductor systems, in particular, are excellent candidates for neuromorphic devices due to their capacity to operate at great speeds and with low energy dissipation compared to their silicon counterparts. In this paper, we revisit a prior work on Josephson Junction-based neurons to identify the exact dynamical mechanisms underlying the system's neuronlike properties and reveal complex behaviors which are relevant for neurocomputation and the design of superconducting neuromorphic devices. Our paper lies at the intersection of superconducting physics and theoretical neuroscience, both viewed under a common framework—that of nonlinear dynamics theory.

DOI: [10.1103/PhysRevE.106.044206](https://doi.org/10.1103/PhysRevE.106.044206)**I. INTRODUCTION**

Neuromorphic computing is a rapidly advancing field that uses neuroscience-inspired concepts to implement circuits of physical neurons. The ultimate goal of neuromorphic computing is the development of powerful algorithms and high-speed, energy-efficient hardware for information processing and the potential acquirement of insight into cognition (for a recent review, see Ref. [1] and references within). The motivation behind the attempt to mimic the brain is its extremely impressive capabilities and advantages as a computing device, in terms of storage, processing speed, memory, and energy consumption.

The reason for its outstanding performance lies in the brain's complexity, specifically the fact that it is dynamic and reconfigurable (due to plasticity)—it provides large interconnectivity, it is stochastic, and exhibits interesting nonlinear phenomena like synchronization and chaos, to mention only a few of the brain's characteristics [2,3]. The latter, in particular, have inspired nonlinear dynamics based computing, which utilizes the many different intrinsic behaviors of a nonlinear dynamical system for performing different types of computation [4,5].

Neuromorphic computing exploits the dynamical and especially the nonlinear-dynamical analogy between many physical systems and neuron biophysics. Various implementations of neuromorphic systems have been proposed, namely, CMOS (complementary metal oxide semiconductor) and memristor devices [6,7], photonic networks [8], spintronic nanodevices [9], and superconductor systems. In light of the recent advances in new materials and hardware, the development of increasingly efficient neuromorphic devices is

challenging yet promising (for a detailed comparison between the aforementioned different approaches, see Ref. [1]).

Superconductor-based neuromorphic systems are particularly advantageous since they are very fast, with operation speeds close to THz, and most importantly, present very low or no power dissipation, even when cryogenic cooling is taken into account. Over the last years, there has been a significant increase in the number of implementations of neuromorphic devices using superconducting elements such as superconducting quantum interference devices (SQUIDs) [10], quantum-phase slip junctions [11], superconducting nanowires [12,13], and Josephson junctions (JJs) [14–18]. The latter produce the so-called single flux quantum pulse [19], which is qualitatively very similar to the action potential that is fired by real neurons when the membrane potential exceeds its threshold.

Most works on JJ neuromorphic devices involve circuit simulations and theoretical modeling (for a recent review, see Ref. [20]). However, several experimental implementations demonstrate that such devices can indeed be fabricated and easily engineered for neuromorphic applications. More specifically, in Ref. [15] a circuit of two mutually coupled excitatory neurons was studied both numerically and experimentally. Each neuron was realized using JJs; a Josephson transmission line acted as the axon and the synapse was modeled by a SQUID similarly to prior works [10]. It was found that the neurons are either desynchronized or synchronized in an in-phase or antiphase state, and that the tuning of the delay and strength of the SQUID synapses can switch the system back and forth in a phase-flip bifurcation [16].

The building block of JJ neuromorphic circuits is the single JJ neuron model, which was developed over a decade ago in Ref. [14]. There it was shown that the JJ neuron is capable of reproducing many characteristic behaviors of biological

*Corresponding author: hizanidis@physics.uoc.gr

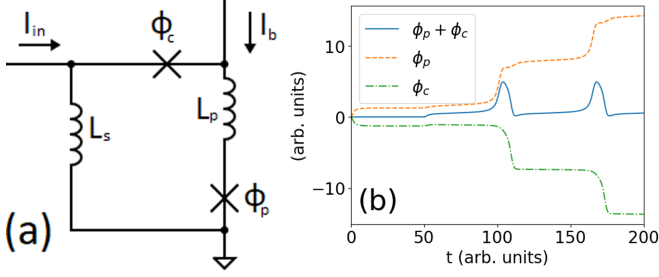


FIG. 1. (a) Circuit diagram for the Josephson Junction neuron. (b) The voltage of the membrane is emulated by the quantity $\phi_p + \phi_c$. Increasing the current from zero to $i_{in} = 0.22$ at $t = 50$ forces the JJ neuron to spike. System parameters: $\Lambda_p = 0.5$, $\Lambda_s = 0.5$, $\lambda = 0.1$, $\Gamma = 1.5$, and $i_b = 1.909$. Initial conditions: $(0,0,0,0)$.

neurons such as action potentials, refractory periods, and firing thresholds. In the present work, we revisit Ref. [14] and perform an extended study on the complex behavior of single JJ neurons to shed light on new dynamics which can further inform the design of devices, and discuss the associated neuro-computational properties this system is capable of presenting. Our work lies at the intersection of superconducting physics and theoretical neuroscience, viewed under the framework of nonlinear dynamics theory.

The paper is organized as follows: In Sec. II, we derive the JJ neuron model and describe the mechanism for the production of the action potential. In Sec. III, the system's complexity is explored through bifurcation analysis and focus is given on its excitable behavior (Sec. III A) and the chaotic and multistable dynamics it presents (Sec. III B). Finally, in Sec. IV, we identify the neuronal properties emulated by the model and stress their significance in terms of neural computation. We summarize our results in Sec. V.

II. JOSEPHSON JUNCTION NEURON MODEL

As implied by its name, the JJ neuron involves two Josephson junctions, in a loop, as shown in the circuit depicted in Fig. 1(a) (where JJs are marked with an X). A JJ is a nonlinear superconducting element made by two superconductors connected through a weak link such as an insulator. The fundamental properties of JJs have been established long ago [21] and have been exploited in numerous applications in superconducting electronics, sensors, and high frequency devices ever since. Each superconductor of the JJ can be described by a single macroscopic wave function with a corresponding phase, and the difference between these two phases is the so-called Josephson phase, denoted by ϕ .

In an ideal JJ, the (super)current through the JJ and the voltage across the JJ are related through the celebrated Josephson relations $I = I_{cr} \sin(\phi)$ and $V = (\hbar/2e)d\phi/d\tau$, where I_{cr} is a critical current above which the voltage develops, τ denotes the time, e is the electron charge, and \hbar is the Planck's constant. Within the framework of the resistively and capacitively shunted junction model [19], the current flowing through the junction is given by Kirchhoff's law and contains contributions from a displacement current and an ordinary current,

represented by a capacitor C and a resistor R , respectively:

$$\frac{\hbar C}{2e} \frac{d^2\phi}{d\tau^2} + \frac{\hbar}{2eR} \frac{d\phi}{d\tau} + I_{cr} \sin \phi = I. \quad (1)$$

The mechanical analog of the JJ is the damped pendulum driven by a constant torque. Depending on the initial conditions, the strength of the drive and the damping, the solution of such a system may involve static tilting, whirling modes, or a combination of the two [22]. In the JJ, the whirling of the phase, when the applied current exceeds a critical value, creates a magnetic flux pulse [19]. This single flux quantum forms the basis for the pulse produced by the JJ neuron model, which is qualitatively very similar to the action potential that occurs in real neurons when the membrane potential exceeds its threshold. A schematic plot of the JJ neuron is shown in the circuit of Fig. 1(a). The two (identical) JJs connected in a superconducting loop are called pulse and control junctions, and are denoted by the subscripts p and c , respectively [14]. By simplifying Eq. (1) using the following normalizations: $t^2 = \tau^2(2eI_{cr}/\hbar C)$, $\Gamma^2 = \hbar/(2eI_{cr}R^2C)$, $i = I/I_{cr}$, and by direct application of Kirchhoff's laws, we obtain the dimensionless equations for the phases of the JJ neuron circuit:

$$\ddot{\phi}_p + \Gamma \dot{\phi}_p + \sin \phi_p = -\lambda(\phi_p + \phi_c) + \Lambda_s i_{in} + (1 - \Lambda_p)i_b, \quad (2)$$

$$\ddot{\phi}_c + \Gamma \dot{\phi}_c + \sin \phi_c = -\lambda(\phi_p + \phi_c) + \Lambda_s i_{in} - \Lambda_p i_b, \quad (3)$$

where the dot notation refers to differentiation with respect to t , Λ_s and Λ_p are the inductances L_p and L_s , respectively, scaled by their sum $L_{tot} = L_s + L_p$, the currents i_b and i_{in} are scaled by the critical current I_{cr} , and, finally, $\lambda = \hbar/(2eL_{tot}I_{cr})$ is the coupling parameter. The bias current i_b provides necessary amounts of energy to both junctions, while the current i_{in} emulates the incoming postsynaptic current received by the neuron.

For appropriate parameter values, the magnetic flux in the JJ neuron $\lambda(\phi_p + \phi_c)$ emulates the voltage difference across the neuronal membrane. In Fig. 1(b), we visualize $\phi_p + \phi_c$, omitting λ because it is just a scaling factor, to demonstrate the generation of the action potential in the JJ neuron. The stimulus i_{in} is sufficiently strong after $t > 50$, so it forces phase ϕ_p to increase abruptly [orange (dashed) curve in Fig. 1(b)]. The coupling between ϕ_p and ϕ_c , regulated by λ , causes the opposite reaction for the phase ϕ_c [green (dotted-dashed) curve in Fig. 1(b)]. The combined effect of the two phases results in the creation of a pulse [blue (solid) curve in Fig. 1(b)] which is qualitatively very similar to the action potential of a real neuron.

The analogy between the JJ neuron and the biological one also extends to the voltage across the pulse and control junctions: ϕ_p and ϕ_c correspond to the ionic currents flowing in real neurons, Na^+ and K^+ , respectively, which underlie the generation of the action potential [23]. After the JJ neuron fires, phase ϕ_p slowly starts to build up again, ϕ_c reacts accordingly (as described previously), and this results in a refractory periodlike behavior before the next spike occurs (Fig. 1(b)). For further details on the creation of the JJ neuron action potential, one may refer to Ref. [14].

As far as design and fabrication is concerned, JJ neurons are based on the widely studied rapid single flux quantum (RFSQ) circuitry [15,24]. The latter provides us with physically meaningful parameter values which typically are the following: For the critical current $I_{cr} \in [10 - 100 \mu\text{A}]$, for the inductances $L_s, L_p \in [1 - 100 \text{pH}]$, the bias and input currents i_b and i_{in} assume values close to I_{cr} , and the junction size, which determines its capacitance C and resistance R (and therefore parameter Γ) is in the range of $0.7 - 5 \mu\text{m}$. Based on these values, we obtain the dimensionless parameters $\lambda = 0.1$ and $\Lambda_p = \Lambda_s = 0.5$, which are kept fixed as in previous works [14–16]. Similarly, the bias current is kept constant at a typically used value $i_b = 1.909$. In the Appendix, we investigate the role of i_b and explain why values close to but lower than 2 should be used. In the following sections, we explore the role of Γ , which remains unaltered after the fabrication of the JJ, and that of i_{in} , which in principle is tunable.

III. DYNAMICS OF THE JJ NEURON

The JJ neuron model described in the previous section reproduces many characteristic properties of biological neurons such as action potentials and firing thresholds [14]. In this paper, we aim to study these properties in a more systematic way, in terms of bifurcation analysis, and explore further the complexity of the system's dynamics and the corresponding neuronal behaviors they relate to.

A. Excitability and bistability

One of the basic dynamical properties of a neuron which is related to the transition between firing and resting states is excitability, i.e., the ability of a neuron to realize a large amplitude change in its membrane voltage, in response to an external stimulus which is above a certain threshold. Excitability is fundamental beyond neurons, in many physical systems, such as semiconductor structures [25,26] and lasers [27]. There are typically two types of excitability, depending on the relationship between the firing frequency and the applied stimulus intensity [28]. The generated action potential in type-I neurons increases with increasing the applied stimulus, whereas type-II neurons exhibit a finite nonzero frequency as periodic firing begins.

The JJ neuron is capable of demonstrating both types of excitability depending on the system parameter values as reported in Ref. [14]. However, a full bifurcation analysis of the system's excitability is missing. In the present paper, we perform a bifurcation analysis and continuation in the relevant parameter space to identify, in detail, the regions of spiking and resting and the transitions between them.

The transition from resting to spiking occurs through the collision of a stable with an unstable fixed point. Equations (A5)–(A6) of the Appendix provide the equilibria and can be used to detect at which i_{in} values they annihilate. The corresponding bifurcation lines that separate the regions of spiking and resting are depicted in Fig. 2 and are analysed in the following.

For $\Gamma > 1$, the transition occurs through a saddle node on an invariant circle (SNIC) bifurcation, marked by the magenta (dotted-dashed) line in Fig. 2. At the bifurcation point

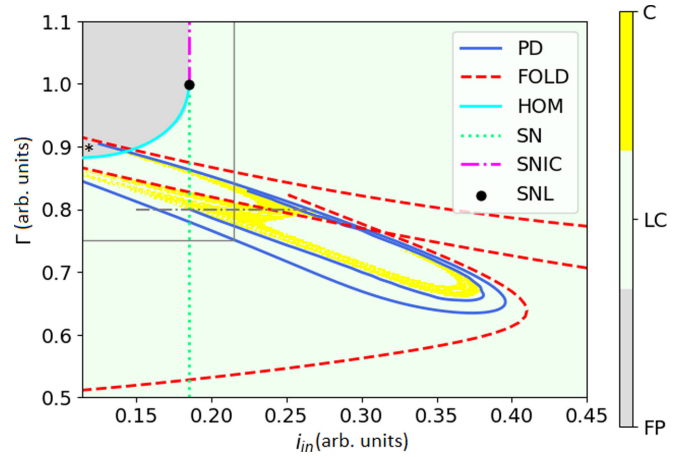


FIG. 2. Chaotic (C), periodic (LC), and resting (FP) dynamics over the parameter plane (i_{in}, Γ) according to the Lyapunov spectrum. The following bifurcation lines are superimposed: period doubling (PD), fold of cycles (FOLD), homoclinic (HOM), saddle node of fixed points (SN), saddle node on invariant circle (SNIC), and saddle-node loop (SNL). The square defined by the gray (light solid) lines and the edges of the graph marks the parameter subspace of Fig. 5 and the light gray (dashed-dotted) horizontal line marks the parameter value range of Fig. 4. The starred area contains fixed points as well as very small periodic and chaotic windows which are not easily visible. Other parameter values: $\lambda = 0.1$, $\Lambda_p = \Lambda_s = 0.5$, $i_b = 1.909$. Different initial conditions were considered, while, in the case of coexistence, we choose to visualize the dynamics as such: C over LC, and LC over FP.

$i_{in,SNIC} = 0.185$, a stable limit cycle is born whose frequency follows the scaling law: $f \sim O(\sqrt{i_{in} - i_{in,SNIC}})$. The square root law is verified by the 0.5 slope in the semilogarithmic plot in the inset of Fig. 3(a), where the frequency of the limit cycle is plotted as a function of the stimulus i_{in} . Exactly at the bifurcation point, the period of the limit cycle is infinite, therefore this bifurcation is also known as saddle-node infinite period bifurcation (SNIPER) and it characterizes neurons of excitability type I [29].

On the other hand, for $\Gamma < 1$, the resting state disappears at a stimulus value $i_{in,SN} = i_{in,SNIC}$ through a saddle-node bifurcation (SN), in this case *off-limit cycle*, marked with a green (light dotted) line in Fig. 2, forcing the trajectories to follow an already existing limit cycle of nonzero frequency. The aforementioned limit cycle is born through a homoclinic (HOM) bifurcation [cyan (light solid) line in Fig. 2] at a stimulus $i_{in,HOM} < i_{in,SN}$. The HOM bifurcation was detected through its characteristic scaling law of the period of the LC near the bifurcation point, which should follow: $T \sim O(\ln[i_{in} - i_{in,HOM}])$. Indeed, the inset of Fig. 3(b), where the limit cycle frequency is plotted over i_{in} , verifies the above relation with an R-squared value of $r^2 = 0.997$. For a fixed Γ value, the JJ neuron is bistable for $i_{in} \in (i_{in,HOM}, i_{in,SN})$, since a limit cycle coexists with a stable equilibrium. This accounts for class-II excitability.

As already mentioned, these bifurcations were detected and identified through the F-I curves which are visualized in Fig. 3. More specifically, we first fixed Γ and then used the following protocol: For each value of the current, the frequency was calculated and the last variable values of the

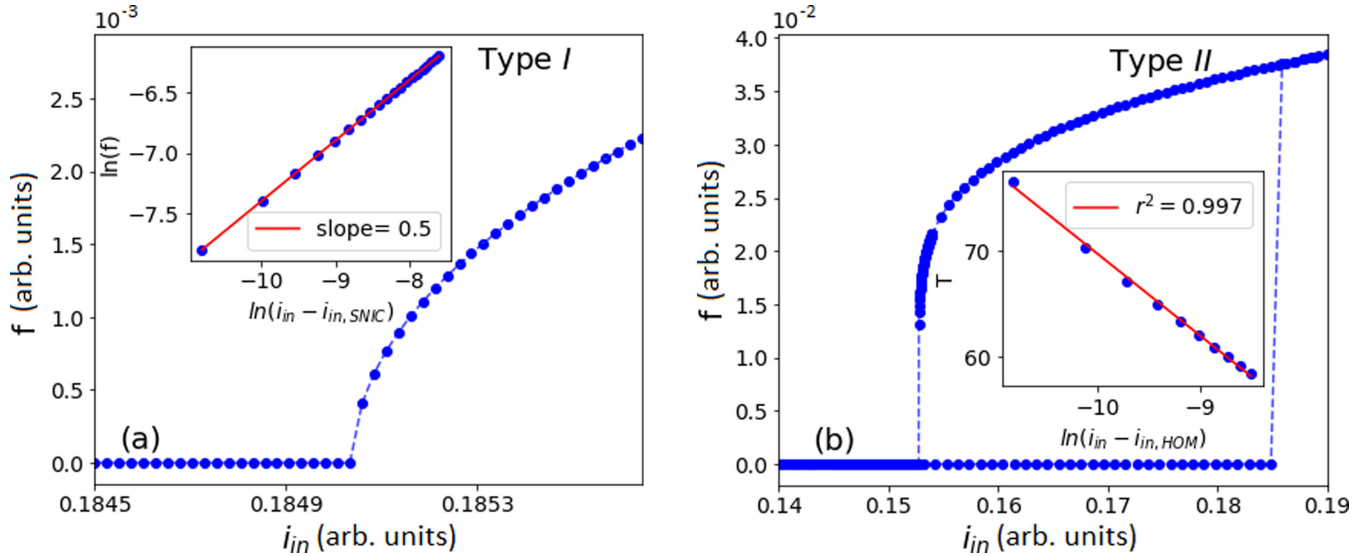


FIG. 3. Frequency of the limit cycle over the stimulus i_{in} : (a) For $\Gamma = 1.5$, spiking occurs through a SNIC bifurcation. (b) For $\Gamma = 0.9$, the curve forms a hysteresis loop between $i_{in,HOM}$ and $i_{in,SN}$ where the neuron either spikes or rests depending on the initial conditions. The inset graphs depict that sample points, near the HOM and SNIC bifurcations, obey the corresponding scaling laws $T_{HOM} \sim O(\ln [i_{in} - i_{in,HOM}])$ and $f_{SNIC} \sim O(\sqrt{i_{in} - i_{in,SNIC}})$, respectively. Other parameters: $\Lambda_p = 0.5$, $\Lambda_s = 0.5$, $\lambda = 0.1$, and $i_b = 1.909$.

trajectory were used as the initial conditions for the next simulation. In this way, the trajectories start at the vicinity of the attractor which was detected in the previous run. In Fig. 3(b), we first increased the current from 0.14 to 0.19 and then moved backward, investigating the current values near the HOM bifurcation.

It can be easily shown that the system is unable to undergo Hopf bifurcations, which are also known to be related with class-II neural excitability. During a Hopf bifurcation, the conjugate pair of two eigenvalues of a fixed point must cross the imaginary axis [30], which is impossible in this system. This stems from Eqs. (A9)–(A12) of the Appendix, which reveal that when the system has complex eigenvalues, their real part is $\text{Re}(e_i) = -\Gamma/2$, which is always a negative quantity and never passes through zero.

At $\Gamma = 1.0$, the two bifurcation points $i_{in,HOM}$ and $i_{in,SN}$ coincide. The process where a saddle-node and a HOM bifurcation coalesce, forming a SNIC bifurcation, is called a saddle node separatrix loop (SNL) or saddle-node HOM orbit bifurcation, marked by a full black dot in Fig. 2. The SNL bifurcation is common to all class-I excitable neurons [31] and has also been found in the single JJ model (see Ref. [32] and references within). To summarize, around the SNL bifurcation, the line $i_{in} = 0.185$ separates spiking from resting behavior. In addition, next to the resting regime, there exists a bistable portion of the parameter space which is bound from above by the HOM bifurcation line. As we move toward lower Γ values in the parameter space, we encounter additional bifurcations, shown in Fig. 2, which lead to more complex dynamics including multistability and chaotic spiking, as we will see in the next section.

B. Chaotic dynamics and multistability

From a mathematical point of view, the JJ neuron is a four-dimensional nonlinear dynamical system and, therefore,

is capable of presenting a plethora of complex phenomena. In this section, we will focus on the chaotic and multistable dynamics exhibited by the system. The chaotic regimes are detected according to the Lyapunov spectrum, which was extracted using the Dynamical Systems JULIA package [33]. The Lyapunov spectrum consists of four Lyapunov exponents L_i , sorted in descending order, with their sum following $\sum_i^4 L_i = \det J = -2\Gamma < 0$, where J is the Jacobian provided in the Appendix [Eq. (A7)].

Since L_4 is always negative, the three largest Lyapunov exponents are sufficient for characterizing the dynamics of the JJ neuron. Figure 2 demonstrates the different dynamical regimes according to the Lyapunov spectrum. More specifically, for (I) $L_{1,2,3} < 0$, the system’s solution is a fixed point (FP, light gray), for (II) $L_1 = 0, L_{2,3} < 0$, the system’s solution is a limit cycle (LC, pale green), while for (III) $L_1 > 0, L_2 = 0, L_3 < 0$, the system exhibits chaotic behavior (C, yellow). For the generation of Fig. 2, we considered different initial conditions whereas, in the case of coexistence of two or more attractors, we visualize the attractor according to the following order: chaos over limit cycle and limit cycle over equilibrium. In addition, two different types of bifurcation lines are superimposed, namely, period doubling (PD) and fold of cycles (FOLD), marked with blue (dark solid) and red (dashed) colors, respectively. The bifurcation lines have been obtained using a very powerful software tool that executes a root-finding algorithm for continuation of periodic solutions [34].

The bifurcation structure of the system is very intricate: The fold and PD bifurcation lines intersect the HOM and saddle-node line discussed in Sec. III A, thus creating two smaller areas, one triangular shape corresponding to bistability and the starred area in Fig. 2, which mostly contains a single fixed point and some very small windows where the FP coexists with a limit cycle or chaos. Moving toward smaller values of Γ , the system’s dynamics becomes much

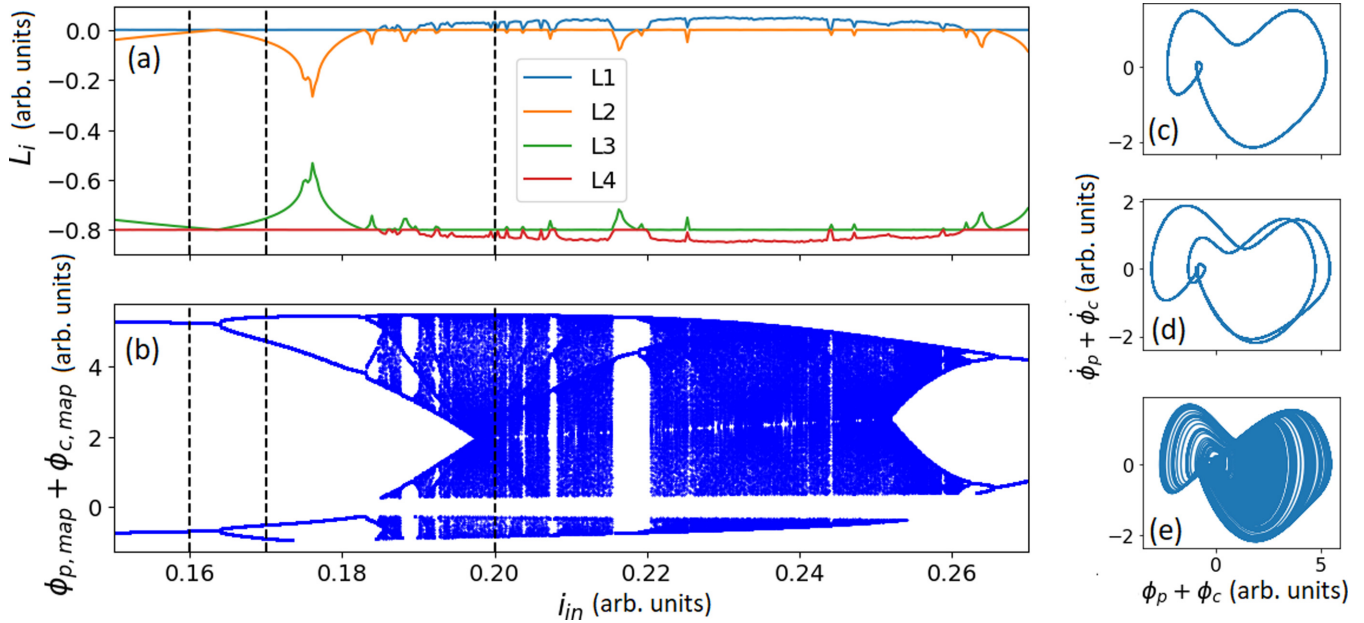


FIG. 4. Route to chaos for $\Gamma = 0.8$: (a) Lyapunov spectrum, (b) orbit diagram of the Poincaré map whose surface of section is the plane $\phi_p + \phi_c = 0$. Dashed lines depict the values of i_{in} which were chosen for the visualization of the phase portraits. More specifically: (c) for $i_{in} = 0.16$, (d) for $i_{in} = 0.17$, and (e) for $i_{in} = 0.20$. Other parameter values: $\lambda = 0.1$, $\Lambda_p = \Lambda_s = 0.5$, $i_b = 1.909$. Each time, the system is initialized close to the attractor detected in the previous run, as in Fig. 3.

more complex and involves multiple periodic solutions which are created and destroyed through fold bifurcations of cycles, as well as oscillatory and chaotic states coexisting with the stable equilibria. From Fig. 2, it is evident that the transition from periodic to chaotic motion takes place through a PD route to chaos [22]. This can be illustrated more clearly if we focus on the cross section of the parameter space for $\Gamma = 0.8$, $i_{in} \in [0.15, 0.27]$, marked by the light gray (dashed-dotted) line in Fig. 2.

The blowup of this region is shown in Fig. 4, where the Lyapunov spectrum as a function of i_{in} is plotted. For $0.15 < i_{in} < 0.1632$, it holds that $L_1 = 0, L_{2,3} < 0$, and the dynamics is, therefore, periodic. At $i_{in} = 0.1632$, the two largest Lyapunov exponents become zero $L_1 = L_2 = 0$ and the first PD bifurcation occurs. This is followed by a cascade of PD bifurcations which lead to chaos, where $L_1 > 0, L_2 = 0, L_3 < 0$. Note that, for simplicity, in Fig. 2, we have only plotted the outer PD line that includes the first PD bifurcation.

The route to chaos is also reflected in the corresponding Poincaré map, shown in Fig. 4, where we store the value $\phi_{p, map} + \phi_{c, map}$ each time the trajectory crosses the plane $\phi_p + \phi_c = 0$ and $\dot{\phi}_p + \dot{\phi}_c < 0$. This particular selection of the variables and plane of intersection is not arbitrary, as the stored quantities are the local maxima of the JJ neuron response. The first simulation of Fig. 4, that is, for $i_{in} = 0.15$, was initialized at $(\phi_{p,0}, \omega_{p,0}, \phi_{c,0}, \omega_{c,0}) = (0, 20.0, 0, 0)$, same as in Fig. 2. The following runs, on the other hand, were initialized with the last variable values of the previous simulation. Thanks to this protocol, we are able to follow the evolution of the attractor which becomes chaotic without falling into the resting state or other LCs. Comparing the Lyapunov spectrum of Fig. 4(a) with the Poincaré map of Fig. 4(b), it is clear that when $L_1 = L_2 = 0$ the branches of the map split in two, which is the signature of the PD bifurcation. This transition to

chaos is also visualized in Figs. 4(c) and 4(d), where the phase portraits in the $(\phi_p + \phi_c, \dot{\phi}_p + \dot{\phi}_c)$ plane are shown, for values of the control parameter i_{in} marked by the vertical dashed lines in Figs. 4(a) and 4(b). At $i_{in} = 0.16$, the system has a period-1 solution [Fig. 4(c)], which doubles its period after the first PD bifurcation [Fig. 4(d)], and consequently undergoes a cascade of PDs before entering chaos [Fig. 4(e)].

To have an overview of the menagerie of behaviors exhibited by the JJ neuron, we have created a mapping of all the different dynamical regimes analyzed above, shown in Fig. 5.

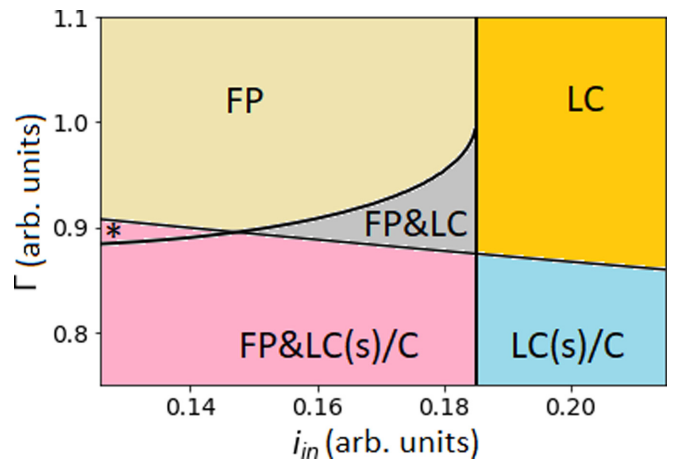


FIG. 5. Different dynamical regimes in the parameter space (i_{in}, Γ) . The detected dynamics are fixed points (FP), limit cycles (LC), chaos (C), and coexistence thereof, in various combinations. The starred area corresponds to the same area in 2 and it mostly contains exclusively a FP and some very small windows of coexistence of a FP and a LC or C. System parameters: $\Lambda_p = 0.5$, $\Lambda_s = 0.5$, $\lambda = 0.1$, and $i_b = 1.909$.

Previous works on JJ neurons focused on regimes where the sole attractor is a periodic orbit [14]. However, the system is capable of presenting a plethora of additional dynamics and the knowledge of its full behavior is useful for the design of experiments based on JJ neurons and particularly their exploitation with relevance to neurocomputation. In principle, different behavior is expected if one explores the parameter space of λ , Λ_s , and Λ_p . Nonetheless, this would be beyond the scope of the present paper since the focus here is the effect of the biologically relevant parameter Γ , which determines the excitability type of the neuron, and i_{in} which models the input currents arriving at the neuron and is easily tunable in an experimental setup.

IV. NEUROCOMPUTATIONAL PROPERTIES OF THE JJ NEURON

The dynamical behavior described in the previous section determines the neurocomputational properties of a JJ neuron. The JJ neuron is known to be capable of reproducing many characteristic behaviors of biological neurons [14]. In this section, we extend these findings by identifying additional neuronal properties emulated by the JJ model and stressing their significance in terms of neural computation.

In Sec. III A, we confirmed via bifurcation analysis that the JJ neuron is capable of mimicking neurons of both classes I and II of excitability. Both classes of excitability have been observed in biological experiments, for instance, in pyramid neurons in the hippocampus and interneurons in the neocortical region, respectively [35,36], among others. Differences in excitability result in differences in spike initiation, which in turn has implications for essential biological functions of the brain such as information encoding and processing [29,37]. Moreover, different classes of neuronal excitability can affect the collective behavior of the nervous system, particularly the phenomenon of synchronization is shown to be achieved more easily in a neuronal network with class-II neurons rather than that with neurons of class I [38].

Regarding the JJ neuron, the key element in the dynamics relating to both classes of excitability is the SNL codimension 2 bifurcation depicted in Fig. 2. This bifurcation is found in other famous neuronal models such as the Morris-Lecar and Wilson-Cowan models [39]. Moreover, it is linked to other neurocomputational properties, namely, the existence of a well-defined threshold, all-or-none behavior, and spike latency [39]. The latter property is related to the bottleneck created at the SNIC and SN bifurcations and refers to the existence of significant delays, which can reach up to a second in real neurons, in the production of the first spike when the stimulus is barely greater than the threshold [40]. Another interesting feature related to the SNL bifurcation is that it governs the transition between the two classes of neuronal excitability. Such transitions have been observed in biological experiments [35] and recently it was reported that they may be induced by autapses [41], i.e., synapses from a neuron onto itself via closed loops.

The neurons we have encountered can be in a quiescent state or they can fire, either regularly or chaotically. When a neuron alternates between these two states, periodically it is said to be bursting. In autonomous bursting, that is, for

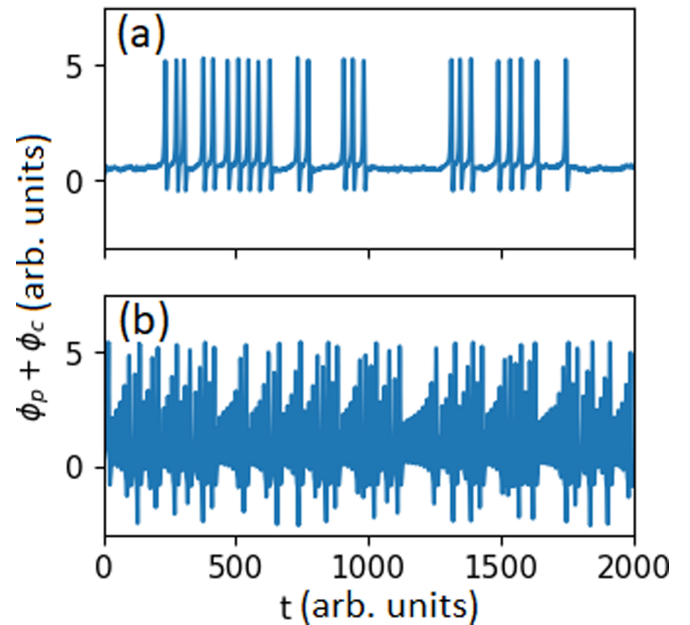


FIG. 6. Different neurocomputational properties of a JJ neuron: (a) Noise-induced bursting for $\Gamma = 0.95$ and stimulus $i_{in} = 0.182 + 0.04\xi(t)$, where $\xi(t)$ is Gaussian white noise, (b) chaotic spiking for $\Gamma = 0.8$ and $i_{in} = 0.2$. Other parameter values: $\lambda = 0.1$, $\Lambda_p = \Lambda_s = 0.5$, $i_b = 1.909$.

constant stimulus, there should generally be an additional variable with a slower timescale than those participating in the spiking, which is responsible for turning off and on the generation of the action potentials [37]. For this reason, even though four-dimensional systems such as the JJ neuron are, in principle, capable of displaying bursting, we have not detected this kind of behavior in our model. The existing model is capable of emulating another type of bursting which is induced by noise rather than some intrinsic mechanism [31]. We should mention at this point that the latter has been achieved in networks of globally coupled mixed populations of oscillatory and excitable JJs [42,43]. Let us now assume a JJ neuron which is in the bistable regime where resting and spiking states coexist. To model the variation of the stimulus due to extrinsic noise present in real neurons [44,45] we incorporate an additive Gaussian white noise term $\xi(t)$ with amplitude of 0.04. The stochastic differential equations were integrated with Milstein's method [46]. The addition of noise helps the system alternate between spiking and quiescence, resulting in a burstinglike behavior as shown in the time-series depicted in Fig. 6(a). Both bistability and bursting behaviors have been found in recordings of biological neurons [37], while the latter is also considered to be linked to a distinct mode of neuronal signaling [47].

In the same figure, we have also plotted the case of chaotic dynamics as we analyzed in Sec. III B. Figure 6(b) displays a typical example of chaotic firing of the JJ neuron for $\Gamma = 0.8$ and $i_{in} = 0.2$. Chaotic behavior in neurons has been extensively studied both in real recordings of neuronal activity [48] and in mathematical models [49], and has been found to be very crucial in terms of cognitive functions. In particular, due to their information-carrying capacity, chaotic attractors may

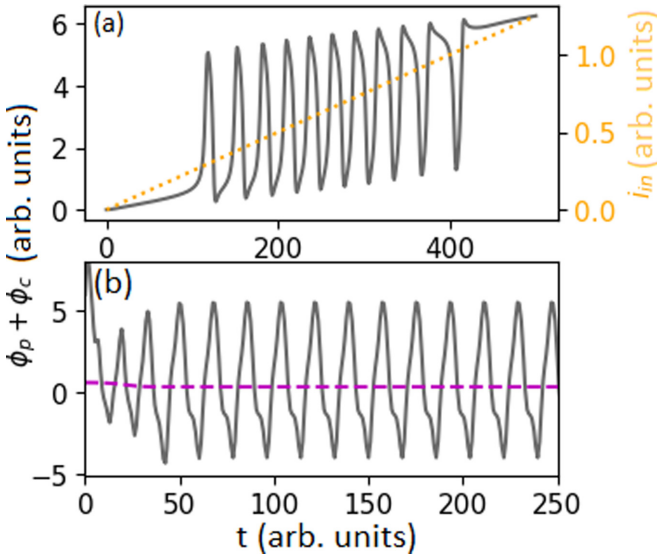


FIG. 7. Behaviors beyond biological relevance: (a) Periodic behavior of equilibria with increasing i_{in} for $\Gamma = 1.5$, (b) Non-spikelike limit cycle depicted in gray (solid) for $\Gamma = 0.7$ and $i_{in} = 0.15$ and a coexisting stable fixed point depicted in magenta (dashed line). Other parameter values: $\lambda = 0.1$, $\Lambda_p = \Lambda_s = 0.5$, $i_b = 1.909$.

serve as information processors and cognitive devices [2,50]. Moreover, chaos and bifurcations can be exploited for nonlinear dynamics based computing [4,5].

Very recently, in Ref. [51], authors discovered that an artificial network of metallic nanowires with synapselike memristive junctions can be tuned to respond in a brainlike way when electrically stimulated. More specifically, they found that by keeping this network of nanowires in a brainlike state at the edge of chaos, it performed tasks at an optimal level. These results suggest that neuromorphic devices can be tuned into regimes with different, brainlike collective dynamics, which may be exploited to optimize information processing.

Finally, we would like to address some behaviors beyond biological relevance found in the JJ neuron which are particularly interesting. First, the equilibria appear and disappear periodically with respect to the stimulus i_{in} and independently of Γ , as shown in the Fig. 8 of the Appendix. In this paper, we have investigated a certain regime of the parameters, that is, for $i_b = 1.909$ and $i_{in} \in [0.0, 0.2]$, where increasing the stimulus results in the disappearance of the stable equilibria. Larger input values, however, such as the ones depicted in Fig. 7(a), may force a spiking neuron to rest, which is not biologically plausible according to our knowledge. Furthermore, Fig. 2 reveals that there are one or more periodic and even chaotic attractors which coexist with the resting states, especially for $\Gamma < 1$. In some cases, these attractors are created or destroyed by means of fold bifurcation of limit cycles or PD bifurcations. For example, Fig. 7(b) shows a periodic solution which does not have the familiar spikelike form.

V. CONCLUSIONS

In summary, JJ neurons are excellent candidates for playing an important part in neuromorphic computing due to

their capacity to operate in great speeds and with low-energy dissipation compared to their silicon counterparts. For this reason, their dynamical behavior must be fully understood and compared with that of biological neurons.

In this paper, we confirmed the existence of a saddle node loop separatrix (SNL) bifurcation which was detected in the relevant parameter plane. The SNL bifurcation has been found in mathematical models of neurons and is linked with many neurocomputational properties such as excitability of class I or II, existence of a well-defined threshold, all-or-none behavior spike latency, and bistability. All these properties have been identified in biological experiments and are linked to essential computational functions of the brain.

Apart from the SNL bifurcation, the model was also found to exhibit chaotic and multistable dynamics. By means of Lyapunov exponent calculations and bifurcation analysis, we have identified that this is achieved through a PD route to chaos mechanism. Chaotic behavior in real neurons has been verified in the laboratory in numerous experiments. This type of behavior is of particular importance, as the brain is thought to operate best at the edge of chaos, i.e., at a critical transition point, between randomness and order. The JJ neuron also exhibits noise-induced bursting, while autonomous bursting could possibly be achieved by coupling the bias current i_b with some other variable of the system, for example, the voltage of the p junction, ϕ_p . A complete mapping of all the possible dynamics presented by the JJ neuron has been created and can be used to inform the design of relevant experiments, where coupling effects are anticipated to give rise to emergent phenomena beyond the dynamics of the single system.

Finally, we also report on other properties of the JJ neuron which are beyond biological relevance such as nonspikelike periodic trajectories and a periodic dependence of the equilibria on the input stimulus. Further investigations of the JJ neuron could involve the implementation of a synapse and the study of the coupled system or, more interestingly, the modeling of excitatory and inhibitory neural autapses.

ACKNOWLEDGMENTS

This paper was supported by the General Secretariat for Research and Innovation (GSRI) and the Hellenic Foundation for Research and Innovation (HFRI) (Code No. 203). D.C. would like to thank Joniald Shena for valuable discussions.

APPENDIX

In the following, we derive expressions for the fixed points of the JJ neuron system and perform a linear stability analysis to determine their stability. Defining $\dot{\phi}_p = \omega_p$ and $\dot{\phi}_c = \omega_c$, the original system of Eqs. (2) and (3) is transformed to

$$\dot{\phi}_p = \omega_p, \quad (\text{A1})$$

$$\dot{\omega}_p = -\Gamma\omega_p - \sin\phi_p - \lambda(\phi_c + \phi_p) + \Lambda_s i_{in} + (1 - \Lambda_p)i_b, \quad (\text{A2})$$

$$\dot{\phi}_c = \omega_c, \quad (\text{A3})$$

$$\dot{\omega}_c = -\Gamma\omega_c - \sin\phi_c - \lambda(\phi_c + \phi_p) + \Lambda_s i_{in} - \Lambda_p i_b. \quad (\text{A4})$$

In this way, the evolution of the system can be visualized as a trajectory in the phase plane $(\phi_p, \omega_p, \phi_c, \omega_c)$. Then the equilibria of the system are $(\phi_p^*, 0, \phi_c^*, 0)$, where ϕ_p^*, ϕ_c^* are provided by solving the following equations:

$$\sin \phi_p^* - \sin \left(-\frac{\sin \phi_p^*}{\lambda} - \phi_p^* + \frac{\Lambda_s i_{in} + (1 - \Lambda_p) i_b}{\lambda} \right) = i_b, \quad (\text{A5})$$

$$\phi_c^* = -\frac{\sin \phi_p^*}{\lambda} - \phi_p^* + \frac{\Lambda_s i_{in} + (1 - \Lambda_p) i_b}{\lambda}. \quad (\text{A6})$$

The next step is to calculate the stability of the equilibria. Thus, the Jacobian was found as

$$J = \begin{bmatrix} 0 & 1 & 0 & 0 \\ -\cos \phi_p - \lambda & -\Gamma & -\lambda & 0 \\ 0 & 0 & 0 & 1 \\ -\lambda & 0 & -\cos \phi_c - \lambda & -\Gamma \end{bmatrix}. \quad (\text{A7})$$

The characteristic equation is given by

$$e^4 + 2e^3 \Gamma + e^2 [\cos \phi_p + \cos \phi_c + 2\lambda + \Gamma^2] + e\Gamma [\cos \phi_p + \cos \phi_c + 2\lambda] + \lambda (\cos \phi_p + \cos \phi_c) + \cos \phi_p \cos \phi_c, \quad (\text{A8})$$

while the roots of Eq. (A8) provide the eigenvalues:

$$e_1 = \frac{1}{2}(-\sqrt{-A+B} - \Gamma), \quad (\text{A9})$$

$$e_2 = \frac{1}{2}(\sqrt{-A+B} - \Gamma), \quad (\text{A10})$$

$$e_3 = \frac{1}{2}(-\sqrt{A+B} - \Gamma), \quad (\text{A11})$$

$$e_4 = \frac{1}{2}(\sqrt{A+B} - \Gamma), \quad (\text{A12})$$

where

$$A = 2\sqrt{(\cos \phi_p - \cos \phi_c)^2 + 4\lambda^2} > 0, \quad (\text{A13})$$

$$B = -2(\cos \phi_p + \cos \phi_c + 2\lambda) + \Gamma^2. \quad (\text{A14})$$

Notice that Γ does not affect the position of the fixed point since it is not contained in Eqs. (A6) and (A5). Moreover, using Eqs. (A9)–(A12), one can show that this is also the case for the sign of the real part of the eigenvalues. Thus, the stability of the equilibria is also independent of Γ . On the

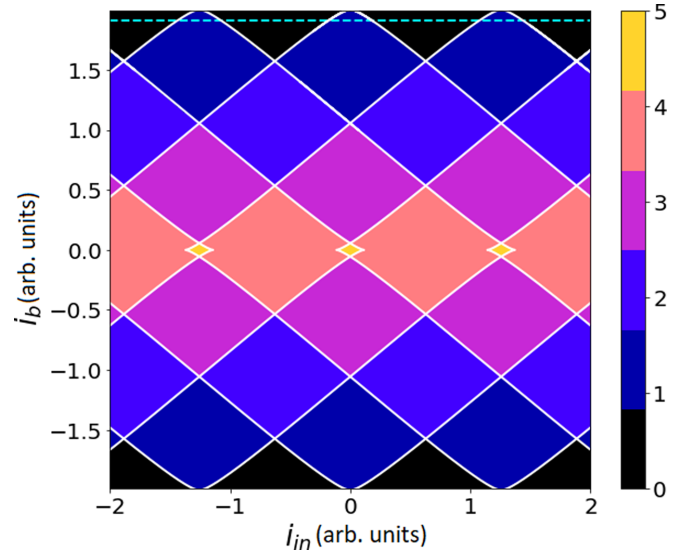


FIG. 8. Number of stable fixed points provided by Eq. (A5) for $i_{in} \in [-2, 2]$ and $i_b \in (-2, 2)$. White lines mark the saddle-node bifurcation. Other parameter values: $\lambda = 0.1$, $\Lambda_p = \Lambda_s = 0.5$. Independent of Γ . The cyan (dotted) line depicts $i_b = 1.909$.

other hand, the value of Γ affects whether the fixed point is a focus, i.e., contains complex eigenvalues, or a node.

Figure 8 shows the number of stable fixed points in the (i_{in}, i_b) parameter plane, while the white lines mark the saddle-node bifurcation lines through which they lose their stability. We observe that the absolute value of i_b affects the number of fixed points more decisively than the stimulus i_{in} . When $|i_b|$ is small, there are many fixed points while when $|i_b| > 2$ there are no equilibria. A typical neuron is expected to rest until the stimulus exceeds a certain threshold value where firing starts. That is why $i_b = 1.909$ was chosen, to ensure spiking behavior. Note, finally, that the graph of Fig. 8 is periodic over the stimulus i_{in} and the borders between different colors mark the annihilation (generation) of fixed points.

Finally, notice that Eqs. (A9)–(A12) reveal the reason why the system does not exhibit Hopf bifurcations. A fixed point can have a pair of complex conjugate eigenvalues only when the radicand is less than zero. During the Hopf bifurcation, the real part of those eigenvalues must cross the real axis. In this case, Γ must flip signs, which is impossible since it corresponds to a positive damping coefficient.

- [1] D. Marković, A. Mizrahi, D. Querlioz, and J. Grollier, Physics for neuromorphic computing, *Nat. Rev. Phys.* **2**, 499 (2020).
- [2] J. S. Nicolis, *Chaos and Information Processing* (World Scientific, Singapore, 1991).
- [3] C. van Vreeswijk and H. Sompolinsky, Chaotic balanced state in a model of cortical circuits, *Neural Comput.* **10**, 1321 (1998).
- [4] F. C. Hoppensteadt and E. M. Izhikevich, Oscillatory Neurocomputers With Dynamic Connectivity, *Phys. Rev. Lett.* **82**, 2983 (1999).

- [5] B. Kia, J. F. Lindner, and W. L. Ditto, Nonlinear dynamics based digital logic and circuits, *Front. Comput. Neurosci.* **9**, 1 (2015).
- [6] V. Milo, G. Malavena, C. M. Compagnoni, and D. Ielmini, Memristive and CMOS devices for neuromorphic computing, *Materials* **13**, 166 (2020).
- [7] T. Birkoben, M. Drangmeister, F. Zahari, S. Yanchuk, P. Hövel, and H. Kohlstedt, Slowfast dynamics in a chaotic system with strongly asymmetric memristive element, *Int. J. Bifurcation Chaos* **30**, 2050125 (2020).

- [8] B. J. Shastri, A. N. Tait, T. F. de Lima, W. H. P. Pernice, H. Bhaskaran, C. D. Wright, and P. R. Prucnal, Photonics for artificial intelligence and neuromorphic computing, *Nat. Photonics* **15**, 102 (2021).
- [9] J. Grollier, D. Querlioz, K. Y. Camsari, K. Everschor-Sitte, S. Fukami, and M. D. Stiles, Neuromorphic spintronics, *Nat. Electron.* **3**, 360 (2020).
- [10] Y. Mizugaki, K. Nakajima, Y. Sawada, and T. Yamashita, Implementation of new superconducting neural circuits using coupled squids, *IEEE Trans. Appl. Supercond.* **4**, 1 (1994).
- [11] R. Cheng, U. S. Goteti, and M. C. Hamilton, Spiking neuron circuits using superconducting quantum phase-slip junctions, *J. Appl. Phys.* **124**, 152126 (2018).
- [12] E. Toomey, K. Segall, and K. K. Berggren, Design of a power efficient artificial neuron using superconducting nanowires, *Front. Neurosci.* **13**, 933 (2019).
- [13] A. E. Lombo, J. E. Lares, M. Castellani, C.-N. Chou, N. A. Lynch, and K. K. Berggren, A superconducting nanowire-based architecture for neuromorphic computing, *Neuromorph. Comput. Eng.* **2**, 034011 (2022).
- [14] P. Crotty, D. Schult, and K. Segall, Josephson junction simulation of neurons, *Phys. Rev. E* **82**, 011914 (2010).
- [15] K. Segall, M. LeGro, S. Kaplan, O. Svitelskiy, S. Khadka, P. Crotty, and D. Schult, Synchronization dynamics on the picosecond time scale in coupled Josephson junction neurons, *Phys. Rev. E* **95**, 032220 (2017).
- [16] Kenneth, S. Guo, P. Crotty, D. Schult, and M. Miller, Phase-flip bifurcation in a coupled Josephson junction neuron system, *Phys. B: Condens. Matter* **455**, 71 (2014); 21st Latin American Symposium on Solid State Physics - SLAFES 2013.
- [17] M. L. Schneider and K. Segall, Fan-out and fan-in properties of superconducting neuromorphic circuits, *J. Appl. Phys.* **128**, 214903 (2020).
- [18] Y. Braiman, B. Neschke, N. Nair, N. Imam, and R. Glowinski, Memory states in small arrays of Josephson junctions, *Phys. Rev. E* **94**, 052223 (2016).
- [19] K. K. Likharev, *Dynamics of Josephson Junctions and Circuits* (Gordon and Breach, New York, 1986).
- [20] M. Schneider, E. Toomey, G. Rowlands, J. Shainline, P. Tschirhart, and K. Segall, Supermind: A survey of the potential of superconducting electronics for neuromorphic computing, *Supercond. Sci. Technol.* **35**, 053001 (2022).
- [21] B. D. Josephson, Possible new effects in superconductive tunnelling, *Phys. Lett.* **1**, 251 (1962).
- [22] S. H. Strogatz, *Nonlinear Dynamics and Chaos with Student Solutions Manual: With Applications to Physics, Biology, Chemistry, and Engineering* (CRC Press, Boca Raton, 2018).
- [23] P. Dayan and L. F. Abbott, *Theoretical Neuroscience: Computational and Mathematical Modeling of Neural Systems* (MIT press, Cambridge, MA, 2005).
- [24] K. K. Likharev and V. K. Semenov, RSFQ logic/memory family: A new Josephson-junction technology for sub-terahertz-clock-frequency digital systems, *IEEE Trans. Appl. Supercond.* **1**, 3 (1991).
- [25] J. Hizanidis, A. Balanov, A. Amann, and E. Schöll, Noise-Induced Front Motion: Signature of a Global Bifurcation, *Phys. Rev. Lett.* **96**, 244104 (2006).
- [26] I. Ortega-Piwonka, O. Piro, J. Figueiredo, B. Romeira, and J. Javaloyes, Bursting and Excitability in Neuromorphic Resonant Tunneling Diodes, *Phys. Rev. Appl.* **15**, 034017 (2021).
- [27] J. L. A. Dubbeldam, B. Krauskopf, and D. Lenstra, Excitability and coherence resonance in lasers with saturable absorber, *Phys. Rev. E* **60**, 6580 (1999).
- [28] A. L. Hodgkin, The local electric changes associated with repetitive action in a non-medullated axon, *J. Physiol.* **107**, 165 (1948).
- [29] J. Rinzel and G. B. Ermentrout, Analysis of neural excitability and oscillations, edited by C. Koch and I. Segev, *Methods in neuronal modeling: From synapses to networks*, 2 ed., (MIT Press, Cambridge, MA, 1998), pp. 251–291.
- [30] Y. A. Kuznetsov, *Elements of Applied Bifurcation Theory*, 2nd ed., Applied Mathematical Sciences (Springer-Verlag, New York, 1998), Chap. 3, pp. 91–104.
- [31] J.-H. Schleimer, J. Hesse, S. A. Contreras, and S. Schreiber, Firing statistics in the bistable regime of neurons with homoclinic spike generation, *Phys. Rev. E* **103**, 012407 (2021).
- [32] S. Schecter, The saddle-node separatrix-loop bifurcation, *SIAM J. Math. Anal.* **18**, 1142 (1987).
- [33] G. Datsis, Dynamical systems.jl: A Julia software library for chaos and nonlinear dynamics, *J. Open Source Softw.* **3**, 598 (2018).
- [34] K. Engelborghs, T. Luzyanina, and D. Roose, Numerical bifurcation analysis of delay differential equations using DDE-BIFTOOL, *ACM Trans. Math. Softw.* **28**, 1 (2002).
- [35] S. A. Prescott, S. Ratt, Y. De Koninck, and T. J. Sejnowski, Pyramidal neurons switch from integrators in vitro to resonators under in vivo-like conditions, *J. Neurophysiol.* **100**, 3030 (2008); PMID: 18829848.
- [36] R. A. Tikidji-Hamburyan, J. J. Martínez, J. A. White, and C. C. Canavier, Resonant interneurons can increase robustness of gamma oscillations, *J. Neurosci.* **35**(47), 15682 (2015).
- [37] E. M. Izhikevich, *Dynamical Systems in Neuroscience: The Geometry of Excitability and Bursting* (MIT press, Cambridge, MA, 2007), Chap. 7, pp. 226–228.
- [38] D. Hansel, G. Mato, and C. Meunier, Synchrony in excitatory neural networks, *Neural Comput.* **7**, 307 (1995).
- [39] E. M. Izhikevich, Neural excitability, spiking and bursting, *Int. J. Bifurcation Chaos* **10**, 1171 (2000).
- [40] E. M. Izhikevich, Which model to use for cortical spiking neurons? *IEEE Trans. Neural Networks* **15**, 1063 (2004).
- [41] Z. Zhao and H. Gu, Transitions between classes of neuronal excitability and bifurcations induced by autapse, *Sci. Rep.* **7**, 6760 (2017).
- [42] C. Hens, P. Pinaki, and K. D. Syamal, Bursting dynamics in a population of oscillatory and excitable Josephson junctions, *Phys. Rev. E* **92**, 022915 (2015).
- [43] A. Mishra, S. Ghosh, S. K. Dana, T. Kapitaniak, and C. Hens, Neuron-like spiking and bursting in Josephson junctions: A review, *Chaos* **31**, 052101 (2021).
- [44] W. Gerstner and W. Kistler, *Spiking neuron models: Single neurons, populations, plasticity*, (Cambridge University Press, Cambridge, 2002).
- [45] N. Brunel, Dynamics of Sparsely Connected Networks of Excitatory and Inhibitory Spiking Neurons, *J. Comput. Neurosci.* **8**, 183 (2000).
- [46] R. Toral and P. Colet, *Stochastic Numerical Methods: An Introduction for Students and Scientists* (John Wiley & Sons, Weinheim, 2014).
- [47] R. Krahe and F. Gabbiani, Burst firing in sensory systems, *Nat. Rev. Neurosci.* **5**, 13 (2004).

- [48] Y. Hirata, M. Oku, and K. Aihara, Chaos in neurons and its application: Perspective of chaos engineering, *Chaos* **22**, 047511 (2012).
- [49] G. Innocenti, A. Morelli, R. Genesio, and A. Torcini, Dynamical phases of the hindmarsh-rose neuronal model: Studies of the transition from bursting to spiking chaos, *Chaos* **17**, 043128 (2007).
- [50] G. Nicolis and V. Basios, *Chaos, Information Processing and Paradoxical Games: The Legacy of John S Nicolis* (World Scientific, Singapore, 2014).
- [51] J. Hochstetter, R. Zhu, A. Loeffler, A. Diaz-Alvarez, T. Nakayama, and Z. Kuncic, Avalanches and edge-of-chaos learning in neuromorphic nanowire networks, *Nat. Commun.* **12**, 4008 (2021).